

# Hydrostatic pressure response of an oxide two-dimensional electron system

J. Zabaleta,<sup>1</sup> V.S. Borisov,<sup>2</sup> R. Wanke,<sup>1</sup> H.O. Jeschke,<sup>2</sup> S.C. Parks,<sup>1</sup> B. Baum,<sup>1</sup> A. Teker,<sup>1</sup>  
T. Harada,<sup>1</sup> K. Syassen,<sup>1</sup> T. Kopp,<sup>3</sup> N. Pavlenko,<sup>1,3</sup> R. Valentí,<sup>2</sup> and J. Mannhart<sup>1</sup>

<sup>1</sup>Max Planck Institute for Solid State Research, 70569 Stuttgart, Germany

<sup>2</sup>Institute of Theoretical Physics, Goethe University, 60438 Frankfurt am Main, Germany

<sup>3</sup>Center for Electronic Correlations and Magnetism,

University of Augsburg, 86135 Augsburg, Germany

(Dated: May 20, 2016)

## Supplementary Material

In the following section we compile figures of measurements and calculations as supporting information to our work.

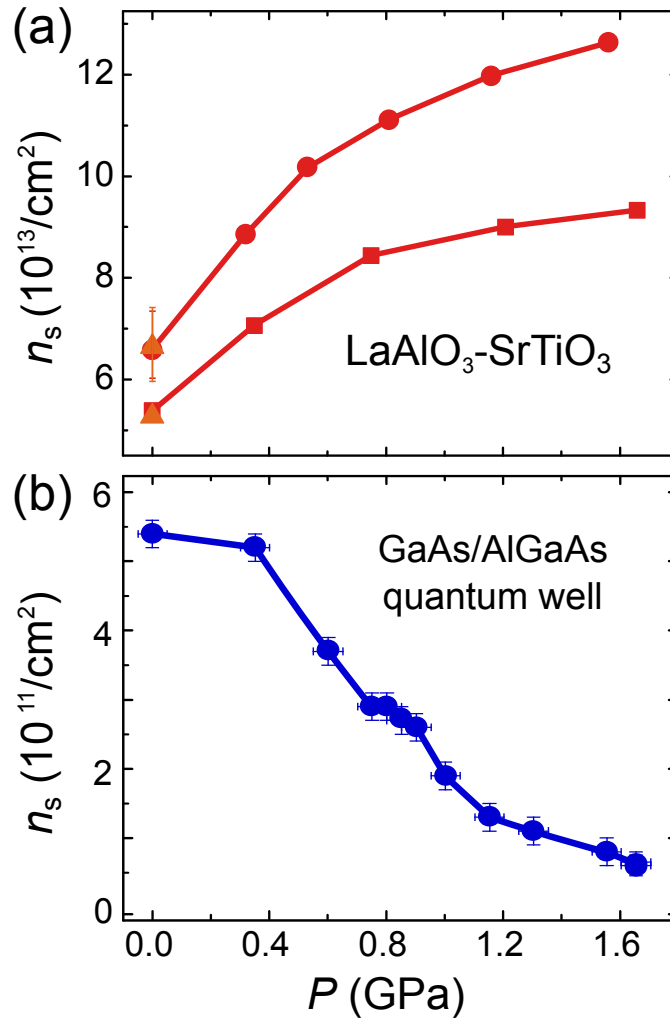
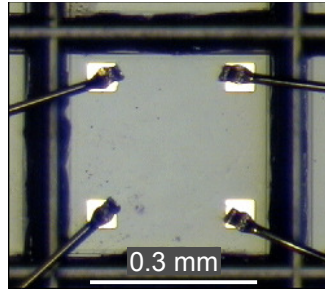


FIG. 1: Effect of pressure on 2D carrier densities: (a) Behavior of the  $\text{LaAlO}_3$ - $\text{SrTiO}_3$  interface compared to (b) a GaAs/AlGaAs single quantum well (data redrawn from Ref. 1). Only error bars that exceed the bullet size are drawn.



$T$ (K)	$R_s$ (k $\Omega$ ) before cut	$R_s$ (k $\Omega$ ) after cut	$n_s$ (cm $^{-2}$ ) after cut	$\mu$ (cm $^2$ /Vs) after cut
300	17	13	$1.1 \times 10^{14}$	4.7
4	0.150	0.157	$3.1 \times 10^{13}$	990

FIG. 2: Optical microscopy image of a cut sample wire bonded for electrical characterization, and table of the electrical characterization results of the assembly at ambient pressure.

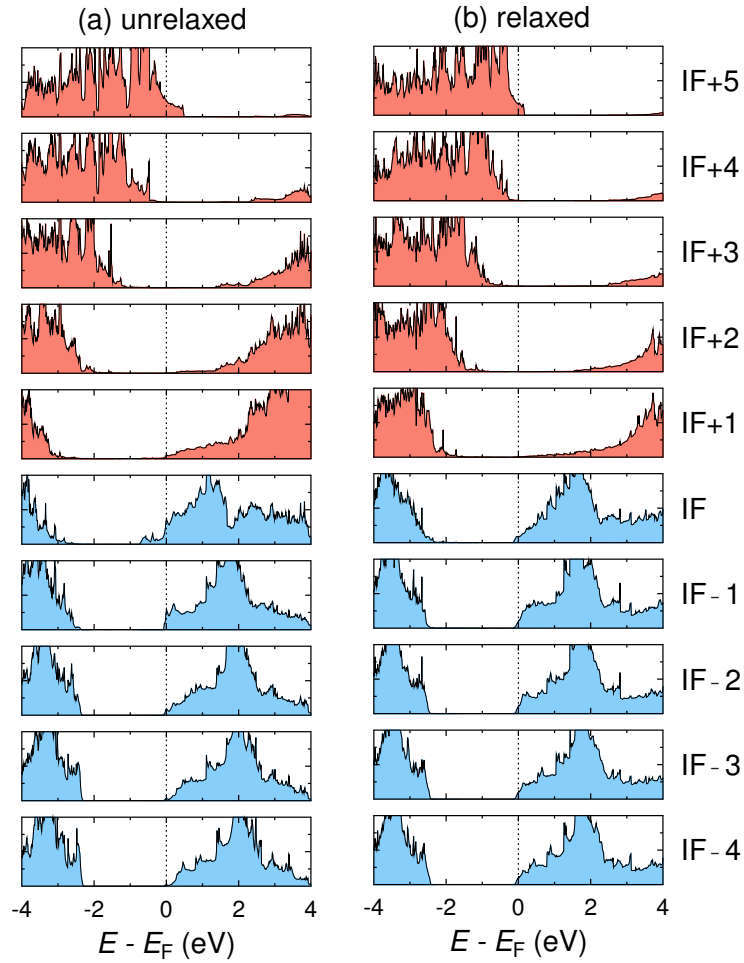


FIG. 3: Unit-cell resolved density of states of the  $(\text{LaAlO}_3)_5/(\text{SrTiO}_3)_{8.5}/(\text{LaAlO}_3)_5$  slab for the unrelaxed (left panel) and structures relaxed internally while keeping the in-plane lattice parameter fixed at  $a_{\perp} = 3.905 \text{ \AA}$  (right panel). Layers are labeled in the same way as in Fig. 3(a) from the main text.

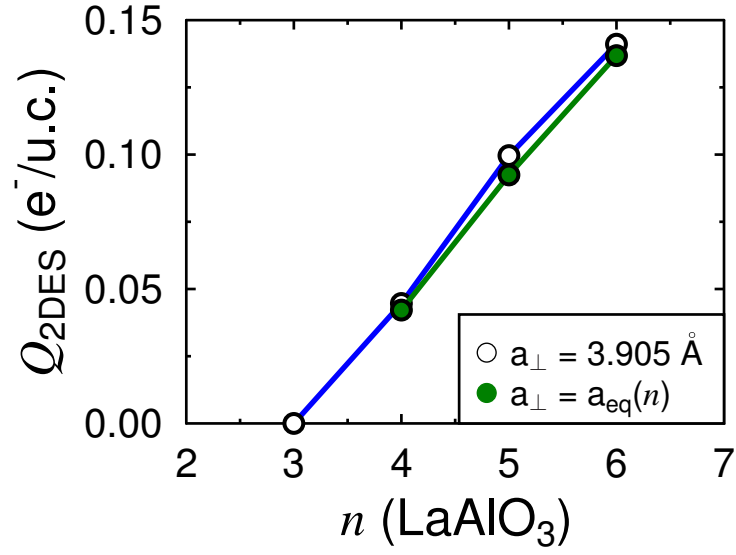


FIG. 4: 2DES density vs. the LaAlO<sub>3</sub> thickness. Filled symbols represent fully relaxed structures with the equilibrium lattice constant  $a_{\text{eq}}$  being a function of  $n$  (number of LaAlO<sub>3</sub> unit cells) and open symbols stand for internally relaxed structures with fixed  $a_{\perp} = 3.905 \text{ \AA}$ . The lines connecting points on the plot are guides to the eye.

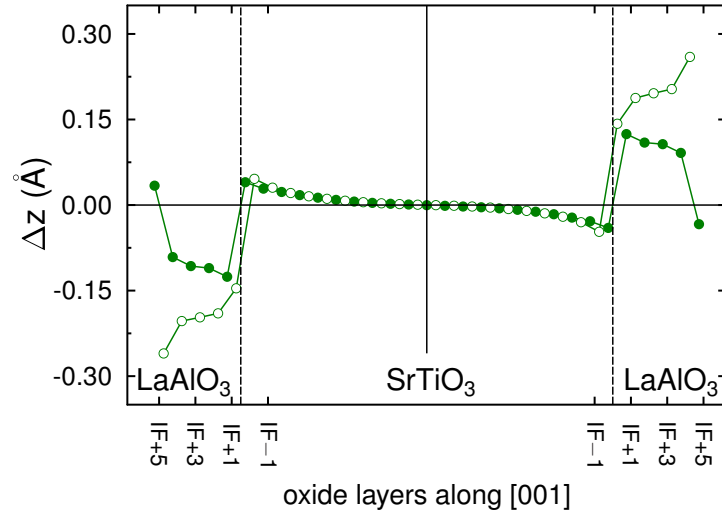


FIG. 5: Ionic displacements in AO ( $A = \text{Sr}, \text{La}$ ; open symbols) and  $\text{BO}_2$  ( $B = \text{Ti}, \text{Al}$ ; filled symbols) oxide layers of the fully relaxed  $(\text{LaAlO}_3)_5/(\text{SrTiO}_3)_{20.5}/(\text{LaAlO}_3)_5$  slab at zero pressure.

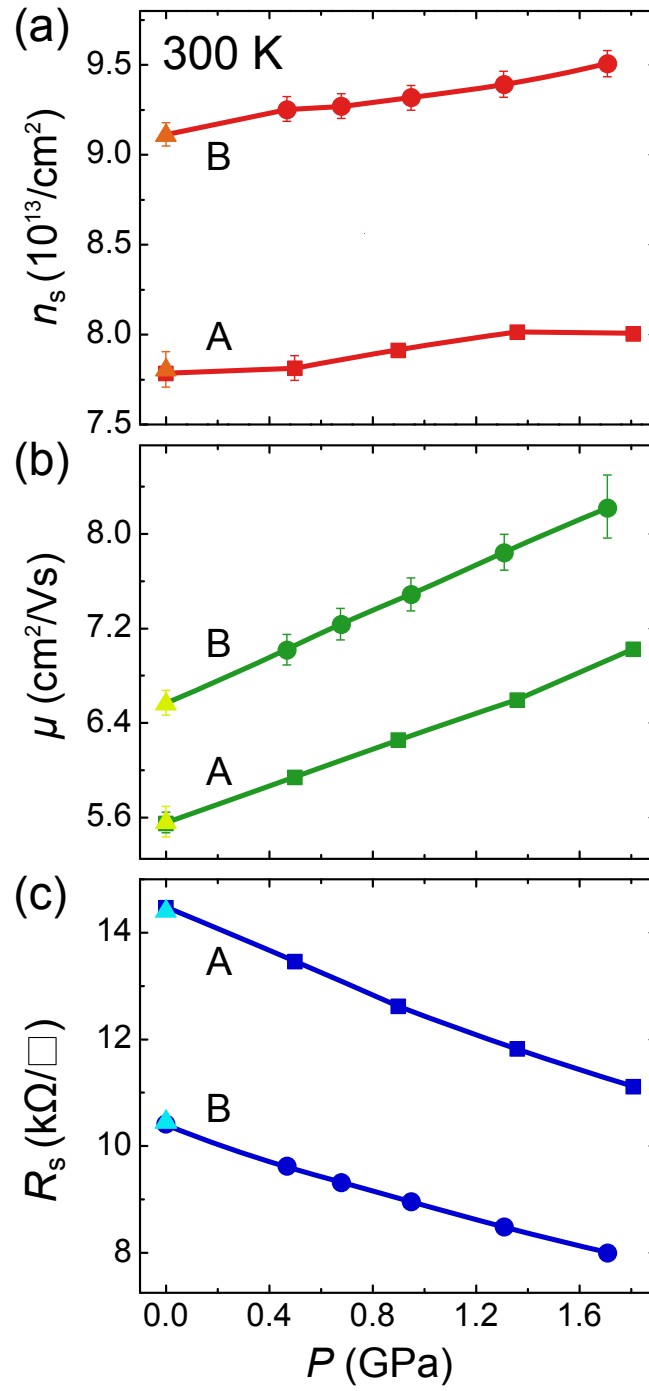


FIG. 6: Transport properties of the LaAlO<sub>3</sub>-SrTiO<sub>3</sub> 2DES as a function of hydrostatic pressure measured at room temperature. Sheet carrier density (a), mobility (b), and sheet resistance (c) of van der Pauw and Hall bar samples as a function of applied pressure. Triangles stand for measurements after unloading the cell. For clarity, only those error bars that exceed the bullet size are drawn. Lines serve as guides to the eye.

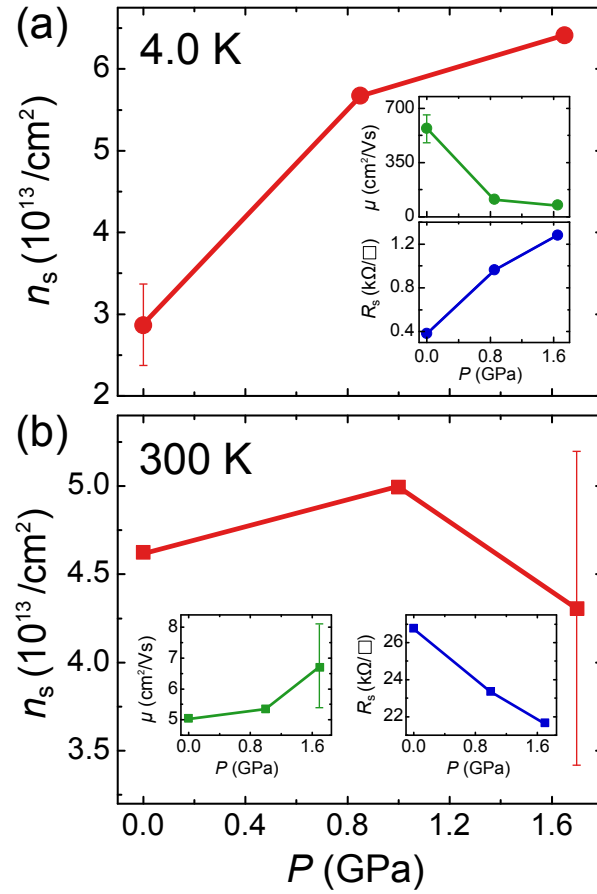


FIG. 7: Transport properties of a  $\text{LaAlO}_3\text{-SrTiO}_3$  2DES in van der Pauw configuration as a function of hydrostatic pressure. This sample showed the largest pressure-induced changes of the sheet carrier density and the carrier mobility at 4 K. The error bars reflect the differences of the results of different magnetic-field sweeps. During the 1.7 GPa warmup a contact deteriorated, resulting in the large error bar of the data point at 300 K, 1.7 GPa. Only error bars that exceed the bullet size are drawn. Lines serve as guides to the eye.

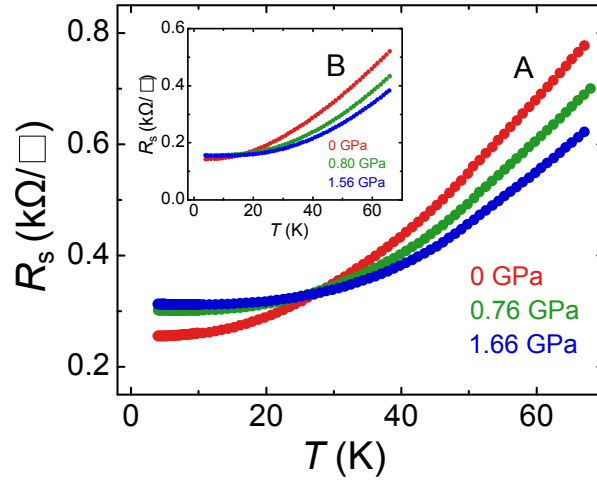


FIG. 8: Sheet resistance of sample A (van der Pauw configuration) and B (Hall bar configuration) measured as a function of temperature for several values of hydrostatic pressure. The two types of samples show similar characteristics.

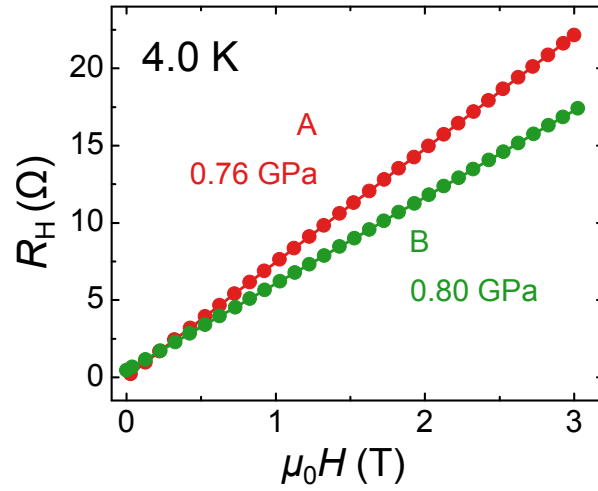


FIG. 9: Hall resistance as a function of the magnetic field measured on two samples (A: 5-unit-cell-thick  $\text{LaAlO}_3$ , van der Pauw; B: 6-unit-cell-thick  $\text{LaAlO}_3$ , Hall bridge) at 4 K under hydrostatic pressure. In order to exclude longitudinal components in the Hall resistance, the values shown here are anti-symmetrized, e.g. we plot the averaged difference between the Hall resistance measured at identical positive and negative magnetic fields.

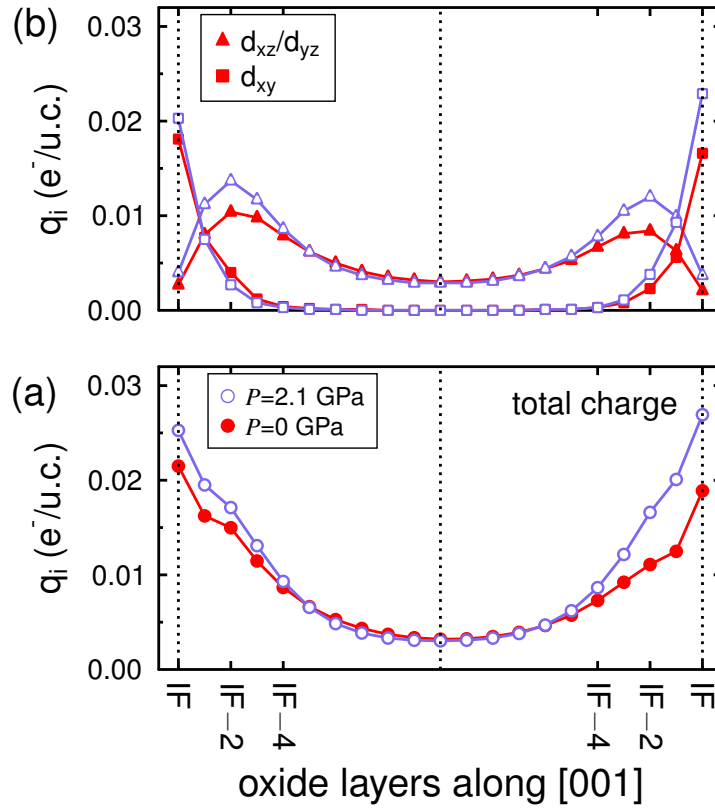


FIG. 10: Charge distribution in the  $\text{SrTiO}_3$  part of the fully relaxed  $(\text{LaAlO}_3)_5/(\text{SrTiO}_3)_{20.5}/(\text{LaAlO}_3)_5$  slab at zero pressure and  $P = 2.1$  GPa. Total electronic charge (a) and its  $d_{xy}$  and  $d_{xz}/d_{yz}$  components (b) are presented.

---

<sup>1</sup> S. Ernst, A. R. Goñi, K. Syassen, and K. Eberl, Collapse of the Hartree term of the Coulomb interaction in a very dilute 2D electron gas, *Phys. Rev. Lett.* **72**, 4029 (1994).